AMERICAN SOCIETY FOR MICROBIOLOGY | Applied and Environmental Microbiology

Environmental Microbiology | Full-Length Text

MmoD regulates soluble methane monooxygenase and methanobactin production in *Methylosinus trichosporium* OB3b

Peng Peng,[1] Junwon Yang,[1] Alan A. DiSpirito,[2] Jeremy D. Semrau[1]

AUTHOR AFFILIATIONS See affiliation list on p. 14.

ABSTRACT Methane oxidation by aerobic methanotrophs is well known to be strongly regulated by the availability of copper, i.e., the "copper switch." That is, there are two forms of methane monooxygenase: a cytoplasmic or soluble methane monooxygenase (sMMO) and a membrane-bound or particulate methane monooxygenase (pMMO). sMMO is only expressed and active in the absence of copper, while pMMO requires copper. Previous work has also shown that one gene in the operon of the soluble methane monooxygenase—*mmoD*—also plays a critical role in the "copper switch," but its function is still vague. Herein, we show that MmoD is not needed for the expression of genes in the sMMO gene cluster but is critical for the formation of sMMO polypeptides and sMMO activity in *Methylosinus trichosporium* OB3b, indicating that MmoD plays a key post-transcriptional role in the maturation of sMMO. Furthermore, data also show that MmoD controls the expression of methanobactin, a copper-binding compound used by some methanotrophs, including *M. trichosporium* OB3b, for copper sequestration. Collectively, these results provide greater insights into the components of the "copper switch" and provide new strategies to manipulate methanotrophic activity.

IMPORTANCE Aerobic methanotrophs play a critical role in the global carbon cycle, particularly in controlling net emissions of methane to the atmosphere. As methane is a much more potent greenhouse gas than carbon dioxide, there is increasing interest in utilizing these microbes to mitigate future climate change by increasing their ability to consume methane. Any such efforts, however, require a detailed understanding of how to manipulate methanotrophic activity. Herein, we show that methanotrophic activity is strongly controlled by MmoD, i.e., MmoD regulates methanotrophy through the post-transcriptional regulation of the soluble methane monooxygenase and controls the ability of methanotrophs to collect copper. Such data are likely to prove quite useful in future strategies to enhance the use of methanotrophs to not only reduce methane emissions but also remove methane from the atmosphere.

KEYWORDS methanotrophy, copper, methane monooxygenase, methanobactin, MmoD

Methanotrophs—microbes that can use methane as their sole carbon and energy source—play an important role in mitigating climate change as methane is a potent greenhouse gas with a global warming potential 28 times higher than that of carbon dioxide over a 100-year time frame (1–4). Perhaps even more importantly, however, is that CH_4 is a short-lived greenhouse gas. As a result, the removal of CH_4 from the atmosphere has the potential to significantly slow near-term climate change. Any such effort to utilize methanotrophs to control methane emissions, however, requires a detailed understanding of the environmental parameters that control methanotrophic activity and how methanotrophs respond to these environmental signals.

Editor Ning-Yi Zhou, Shanghai Jiao Tong University, Shanghai, China

Address correspondence to Jeremy D. Semrau, jsemrau@umich.edu.

The authors declare no conflict of interest.

See the funding table on p. 14.

Received 12 September 2023
Accepted 10 October 2023
Published 28 November 2023

The first and perhaps most crucial step for methane metabolism by aerobic methanotrophs is the oxidation of methane to methanol by methane monooxygenase (MMO). There are two forms of MMO—a membrane-bound or particulate MMO (pMMO) and a cytoplasmic or soluble MMO (sMMO) (5–9). pMMO is found in most aerobic methanotrophs, while sMMO is only found in some methanotrophs (3, 10). Moreover, several methanotrophic species, e.g., *Methylosinus trichosporium* OB3b and *Methylococcus capsulatus* Bath (among others), can express both pMMO and sMMO (7, 11). In these methanotrophs, the expression and activity of the two forms of MMO are controlled according to copper availability, i.e., the "copper switch." sMMO is only expressed and active in the absence of copper, while in the presence of copper, sMMO expression is repressed. Conversely, pMMO expression and activity increase with increasing availability of copper (8, 11, 12).

Intriguingly, although there is a great deal known about the structure and genetics of pMMO, there is a still significant amount of debate as to how this form of MMO oxidizes methane. That is, although pMMO is known to be composed of three subunits, α, β, and γ, encoded by *pmoB*, *pmoA*, and *pmoC*, the number and composition of metal centers in pMMO, as well as the mechanism of methane oxidation, are still contested. Originally, work spearheaded at Northwestern argued that pMMO contained one monocopper site, a dicopper site (both within the soluble regions of PmoB), and a zinc site (in the membrane region of PmoC), and that methane oxidation may occur at either the dicopper or zinc site. Subsequently, this group asserted that methane oxidation occurred at the dicopper site, but further study showed that this putative dicopper center was rather a monocopper center and that methane oxidation likely did not occur there. Rather, it is now argued by this group that methane oxidation may occur at the "original" zinc site and that it actually does not contain zinc, but one, possibly two, monocopper center at this location, and these are coordinated by residues from PmoC and/or PmoA (13–18). Another model of pMMO argues that it contains a tri-copper cluster coordinated by amino acid residues of PmoA and PmoC that serves as the active site (19, 20). Finally, others contend that methane oxidation by the pMMO occurs via a diiron metal complex in the "original" zinc site. This diiron site is coordinated by residues from PmoA and PmoC, and electrons are postulated to be shuttled to this center via a monocopper site (21). It should be stressed that although there is still a great deal of controversy regarding the role and location of copper in pMMO, all models agree that copper is important for the activity of pMMO.

Alternatively, sMMO relies on iron for methane oxidation (6, 7, 22–24). sMMO consists of three components encoded by the *mmo* gene cluster: (i) *mmoXYZ* encoding for the α, β, and γ subunits, respectively, of the sMMO hydroxylase (MMOH) that contains a diiron active site where methane is oxidized (note that this diiron center is very similar to that proposed for pMMO by some researchers (21); (ii) *mmoC* encoding for a reductase that receives electrons from NADH; and(iii) *mmoB* that encodes an electron shuttle protein that enables sMMO to act as an oxygenase and not an oxidase (6, 25, 26) (Fig. 1). To initiate methane catalysis, two electrons are delivered from MmoC to the diiron center of MMOH, reducing the diiron center from a diferric state to a diferrous state. MmoB binds to MMOH and mediates the transfer of electrons to the active site of MMOH where methane and oxygen are bound (6, 27–30).

The *mmo* gene cluster includes an additional gene, *mmoD*, that does not encode for a polypeptide found in the sMMO complex and is not involved in the catalysis of sMMO (Fig. 1) (6, 25). *In vitro* biochemical analysis indicates MmoD can bind to MMOH and act as a potent inhibitor of sMMO (32). Structural analysis indicates that MmoD and MmoB recognize the same binding site of MMOH, and the binding of either MmoD or MmoB to MMOH leads to inhibition or activation, respectively, of MMOH (33). Besides behaving as an inhibitor of MMOH, other work indicates that MmoD may bind DNA and that MmoD is a regulatory protein involved in regulating the expression of pMMO/sMMO, i.e., it plays a role in the canonical "copper switch" of methanotrophs (34).

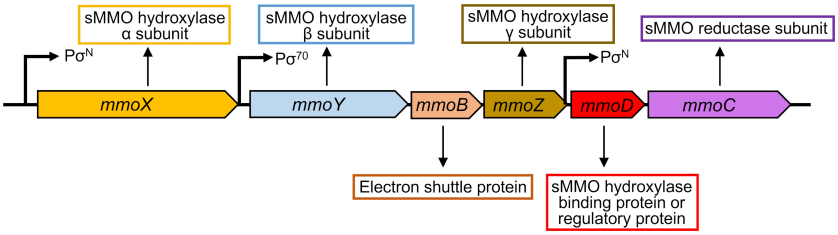

FIG 1 *mmo* gene cluster of *M. trichosporium* OB3b. The protein encoded by each gene and the σ promoter (Pσ) region are indicated in the gene cluster. The sigma promoter upstream of *mmoD* was detected using the Promoter Calculator Tool (31).

Despite these efforts, relatively little is known about MmoD, and there is still some uncertainty as to the number and nature of roles it may play in affecting methanotrophic physiology. For example, is MmoD critical for the formation/assembly of sMMO and methanotrophic growth in the absence of copper? Is MmoD involved in the regulation of other genes besides *pmo* and *mmo*? In this study, we further investigated the function of MmoD in controlling gene expression, physiology, and proteome of *M. trichosporium* OB3b through the construction of a markerless deletion of *mmoD*.

RESULTS

Deletion of *mmoD* gene in *M. trichosporium* OB3b and back complementation in *trans*

To explore the function of *mmoD* in *M. trichosporium* OB3b, a markerless deletion of *mmoD* was constructed (Δ*mmoD*, with 300 bp of *mmoD* deleted, or 80% of the gene sequence, Fig. S1). The absence of *mmoD* in the genome of *M. trichosporium* OB3b was verified by PCR (Fig. S2) and sequencing (data not shown).

To further confirm the function of *mmoD*, a back complementation mutant in *trans* was constructed by cloning *mmoD* and its promoter into pTJS-140 vector and transformed into Δ*mmoD*. Back complementation of *mmoD* in Δ*mmoD* (Δ*mmoD*+pTJS-mmoD) was verified by PCR and kanamycin resistance of Δ*mmoD*+pTJS-mmoD (Fig. S2).

Growth of wild-type *M. trichosporium* OB3b, Δ*mmoD*, and Δ*mmoD*+pTJS-*mmoD* strains

In the absence of copper, the growth of wild-type *M. trichosporium* OB3b was stable for three consecutive transfers in NMS medium, i.e., growth rate (~1.5 d^{-1}) and final OD_{600} (0.6–0.7) for each transfer were comparable and not significantly different (Fig. 2A, G, and H; note that data in Fig. 2G and H also include growth in the presence of copper). In contrast, the growth of Δ*mmoD* in the absence of copper was significantly reduced (P = 0.00006) after the first transfer (1.3 d^{-1} in the first growth cycle to 0.3–0.4 d^{-1} for the second and third cycles; Fig. 2C and H). In addition, the final OD_{600} of Δ*mmoD* was approximately one-third that of wild-type *M. trichosporium* OB3b, despite incubating Δ*mmoD* for approximately twice as long (P = 0.002) (Fig. 2G). More robust growth of Δ*mmoD* in the first cycle was likely due to the transfer of copper from the initial inoculum (this strain was normally maintained in copper-containing growth medium), but such copper contamination was diluted in the second and subsequent transfers. Growth recovered in the Δ*mmoD* strain back-complemented with *mmoD* in *trans* (pTJS-*mmoD*), and the final OD_{600} of each transfer (~0.7) was similar to wild type (Fig. 2E and G). The growth rate of Δ*mmoD*+pTJS-*mmoD* was significantly higher (0.6 vs 0.3 d^{-1}) than Δ*mmoD* but was also significantly lower than the growth of wild-type *M. trichosporium* OB3b (0.6 vs 1.5 d^{-1}) (Fig. 2H).

In the presence of 1 µM copper, the growth of wild-type *M. trichosporium* OB3b, Δ*mmoD,* and Δ*mmoD*+pTJS-*mmoD* strains was comparable for all cycles (growth rate ~1.6 d^{-1}, final OD_{600} ~0.8) (Fig. 2B, D, F, G, and H). Interestingly, the growth rate and

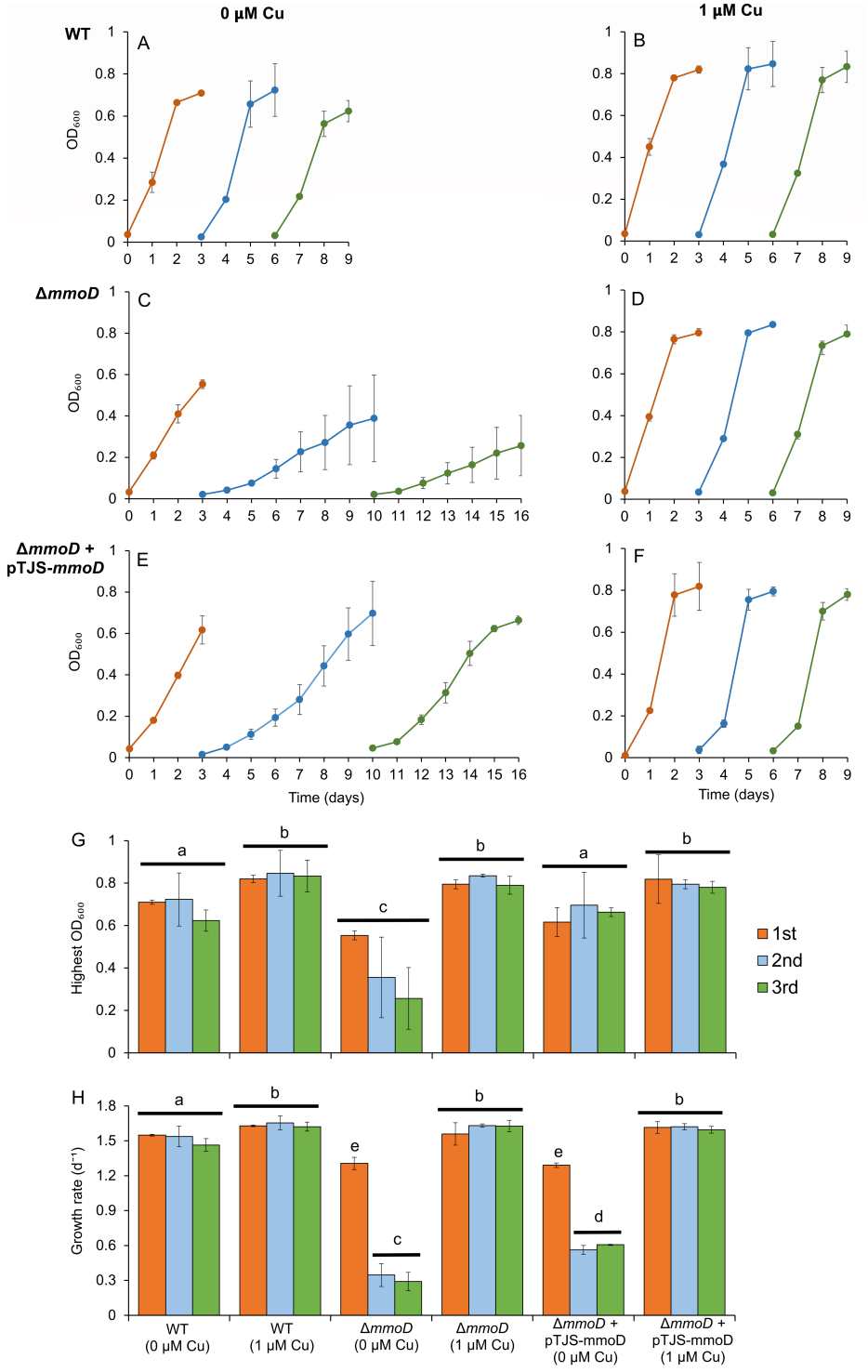

FIG 2 Consecutive transfer and growth of wild-type *M. trichosporium* OB3b (WT), Δ*mmoD*, and Δ*mmoD* with pTJS-*mmoD* in NMS medium without copper (A, C, E) and with 1 μM copper (B, D, F). Highest OD_{600} (G) and growth rate (H) in each transfer were measured and calculated. Error bars indicate standard deviations from triplicate biological cultures. The one-way ANOVA test was performed for variance analysis of the growth rate and OD_{600} between different transfers and growth conditions of wild-type *M. trichosporium* OB3b, Δ*mmoD*, and Δ*mmoD* with pTJS-*mmoD*. Bars within each plot labeled by different letters are significantly different ($P < 0.05$).

final OD_{600} of all strains were significantly higher when grown in the presence of copper vs the absence of copper (final OD_{600}: 0.8 vs 0.3–0.7, growth rate 1.6 vs 0.3–1.5 d^{-1}, $P < 0.05$, Fig. 2G and H).

sMMO activity

Due to the growth inhibition observed in *M. trichosporium* OB3b Δ*mmoD* when grown in the absence of copper, we suspected that the deletion of *mmoD* reduced sMMO activity. sMMO activity was only detected in wild-type *M. trichosporium* OB3b and Δ*mmoD*+pTJS-*mmoD* strains but not in Δ*mmoD* in the absence of copper (Fig. 3A).

Transcriptional analysis of MMO encoding genes and genes involved in copper uptake

RT-qPCR of *mmoX, mmoC,* and *mmoD* was performed to quantify the expression of sMMO genes. *mmoX* expression was over four orders of magnitude higher in the absence vs in the presence of copper for all three strains, i.e., wild-type *M. trichosporium* OB3b, Δ*mmoD,* and Δ*mmoD*+pTJS-*mmoD* (Fig. 3B). No significant difference in *mmoX* expression was observed between wild-type *M. trichosporium* OB3b, Δ*mmoD*, and Δ*mmoD* with pTJS-*mmoD* when grown under the same condition (i.e., with or without 1 µM copper) (Fig. 3B). *mmoC* expression in all the strains was similar to each other, i.e., *mmoC* expression was 50–100-fold higher in the absence of copper than in the presence of 1 µM copper (Fig. 3C). Moreover, *mmoD* expression was over three orders of magnitude higher in the absence vs presence of copper in wild-type *M. trichosporium* OB3b (Fig. 3D). The expression level of *mmoD* decreased less in the absence vs presence of copper for Δ*mmoD*+pTJS-*mmoD* (~3× decrease), but such a difference was significant ($P < 0.003$). In the absence of copper, *mmoD* expression was 10-fold higher ($P = 0.006$) in wild-type *M. trichosporium* OB3b than that observed in Δ*mmoD*+pTJS-*mmoD*. Conversely, in the presence of copper, the expression of *mmoD* was significantly lower (~70 fold) in wild-type *M. trichosporium* OB3b vs Δ*mmoD*+pTJS-*mmoD* (Fig. 3D).

pMMO expression was also monitored by RT-qPCR of *pmoA*. In the absence of copper, *pmoA* expression in wild-type *M. trichosporium* OB3b and Δ*mmoD* and Δ*mmoD*+pTJS-*mmoD* was without any significant difference (Fig. 3E). In the presence of 1 µM copper, *pmoA* expression increased 3–9× in all three strains, and such increase was significant for wild-type *M. trichosporium* OB3b and Δ*mmoD* strains, but not for the back-complemented mutant (Δ*mmoD*+pTJS-*mmoD*). There was little difference, however, in the expression of *pmoA* in the presence of copper for all three strains.

Intriguingly, *mbnA* [encoding the precursor polypeptide of a copper chelating compound, methanobactin (MB)] expression is different in *M. trichosporium* OB3b Δ*mmoD* and Δ*mmoD*+pTJS-*mmoD* as compared to wild-type *M. trichosporium* OB3b. In each of these three strains, *mbnA* expression was 10- to 40-fold higher in the absence vs presence of 1 µM copper. However, in the absence of copper, *mbnA* expression was 22- to 35-fold higher in Δ*mmoD* and Δ*mmoD*+pTJS-*mmoD* than wild-type *M. trichosporium* OB3b (Fig. 3F). In contrast to *mbnA*, two other genes of the *mbn* operon (*mbnB* and *mbnN*, involved in processing the precursor peptide encoded by *mbnA*) did not show significant differences in expression among the three strains in the absence of copper (Fig. S3).

UV-Vis spectroscopy analysis of methanobactin production

Due to the higher expression of the methanobactin precursor gene—*mbnA*—in Δ*mmoD* and Δ*mmoD*+pTJS-*mmoD*, we measured and compared the production of methanobactin in wild-type *M. trichosporium* OB3b, Δ*mmoD,* and Δ*mmoD*+pTJS-*mmoD* via UV-Vis spectroscopy. Absorbances at 340 and 394 nm (associated with the two oxazolone rings critical for binding copper) increased over 2.4-fold in *M. trichosporium* OB3b Δ*mmoD* vs wild type, but only ~1.7-fold when comparing *M. trichosporium* OB3b Δ*mmoD*+pTJS-*mmoD* vs wild type (Fig. 4). These data indicate a much higher MB production in Δ*mmoD*

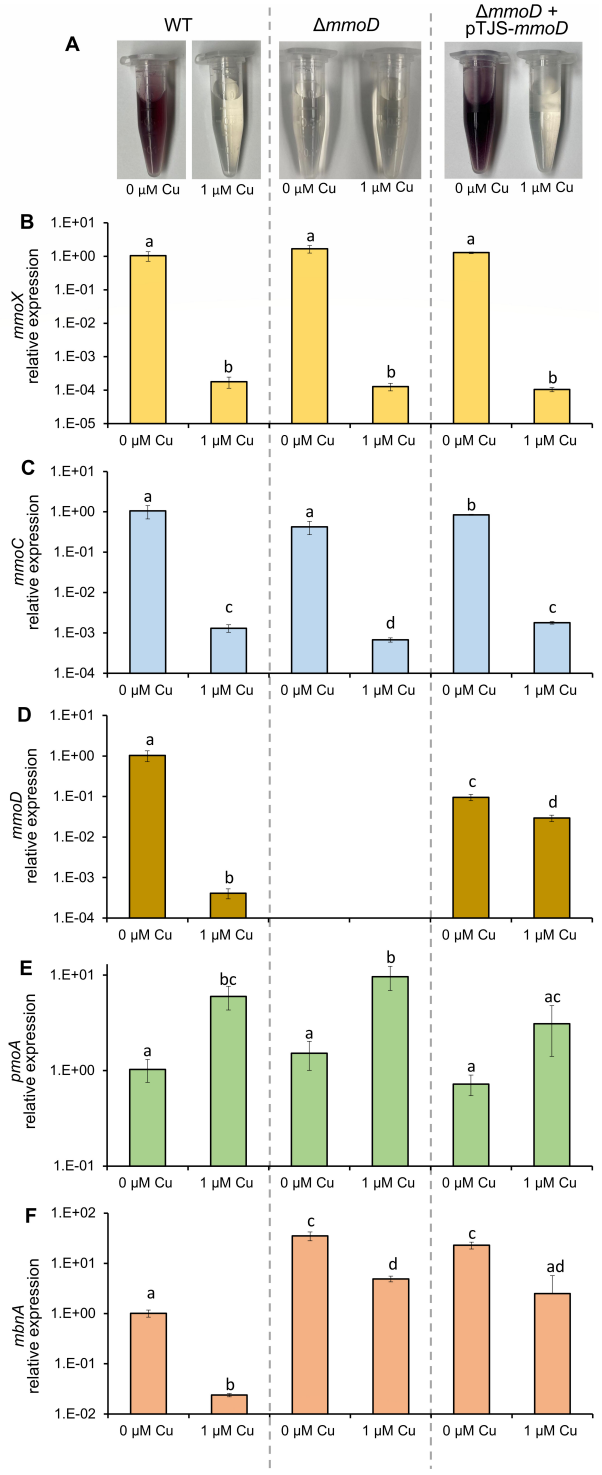

FIG 3 Naphthalene assay of sMMO activity (A) and RT-qPCR analysis of the relative expression of *mmoX* (B), *mmoC* (C), *mmoD* (D), *pmoA* (E), and *mbnA* (F) in wild-type *M. trichosporium* OB3b (WT) (left panel), Δ*mmoD* (middle panel), and Δ*mmoD* with pTJS-*mmoD* (left panel) grown with and without 1 μM copper. Error bars indicate standard deviations from triplicate biological cultures. A *t*-test was performed for variance analysis between wild-type *M. trichosporium* OB3b and Δ*mmoD* under different growth conditions. Bars within each plot labeled by different letters are significantly different ($P < 0.05$).

and Δ*mmoD*+pTJS-*mmoD* strains than wild-type *M. trichosporium* OB3b, which is in line with the transcription of *mbnA* (Fig. 3F).

Proteomic analyses

To further investigate the role of MmoD in the physiology of *M. trichosporium* OB3b, the proteome of wild-type *M. trichosporium* OB3b, Δ*mmoD*, and Δ*mmoD*+pTJS-*mmoD* strains was characterized when grown in the absence of copper. In total 2,411, 2,450, and 2,421 proteins were identified in at least two of three replicate samples of wild-type *M. trichosporium* OB3b, Δ*mmoD*, and Δ*mmoD*+pTJS-*mmoD*, respectively (Fig. S4; Tables S1 to S3). Of these proteins, 44 proteins were found to be differentially expressed ($|\log_2$ fold change$| > 2$, adjusted $P < 0.05$) in *M. trichosporium* OB3b Δ*mmoD* vs wild type, including polypeptides of sMMO—MmoX, Y, Z, and B being significantly lower in the Δ*mmoD* strain [although we should stress expression of *mmo* genes was not different between these strains (Fig. 5; Table S4)]. MmoC, although not significantly different between *M. trichosporium* OB3b Δ*mmoD* vs wild type using our cutoff criteria, did show a $\log_2$ fold change of −1.42, with an adjusted *P* value of 3×10^{-5} (Table S4). Polypeptides for conversion of the methanobactin precursor polypeptide to mature methanobactin (MbnB, C, and N) were not found to have differential abundance in *M. trichosporium* Δ*mmoD* vs wild-type *M. trichosporium* (Table S4), which agrees with the transcriptional results for *mbnB* and *mbnN* (Fig. S3). It should be stressed that the precursor polypeptide of MB—MbnA—was not found in any sample, presumably due it being modified to MB, and thus unable to be detected using standard proteomic methodologies.

When *M. trichosporium* OB3b Δ*mmoD* was back-complemented in *trans*, MmoD was apparent, but less than that observed in wild-type *M. trichosporium* OB3b (~16-fold lower; Table S5). In addition, sMMO polypeptides (MmoXYB and C) in *M. trichosporium* OB3b Δ*mmoD*+pTJS-*mmoD*, although ~1.5–6× lower than that observed in wild-type *M. trichosporium* OB3b, were substantially higher than that observed in *M. trichosporium* O3b Δ*mmoD,* i.e., ~2–16-fold higher (Table S6).

DISCUSSION

Unlike methanotrophs that only express pMMO, e.g., *Methylomicrobium album* BG8 and *Methylocystis* sp. strain SB2 (35, 36), *M. trichosporium* OB3b can survive, if not thrive, in the absence of copper due to the expression of sMMO under low copper (<0.2 µM) conditions (11, 36, 37), aka, the "copper switch." Although the importance of copper

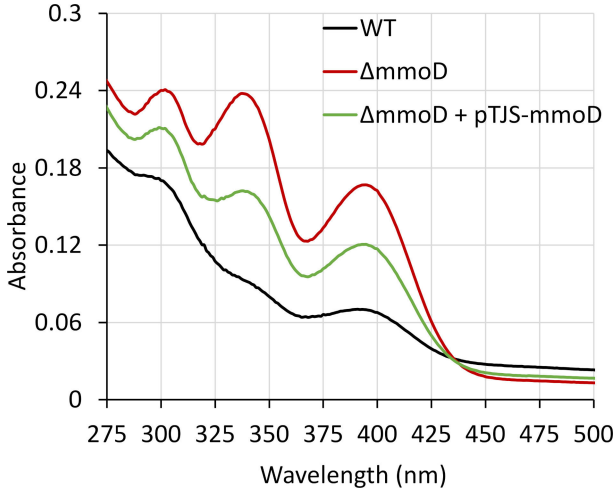

FIG 4 UV-Vis absorption spectra of the supernatant of wild-type *M. trichosporium* OB3b (WT, black), Δ*mmoD* (red), and Δ*mmoD* with pTJS-*mmoD* (green) cultures growing without copper. The OD_{600} of the active growing culture of these strains was ~0.6.

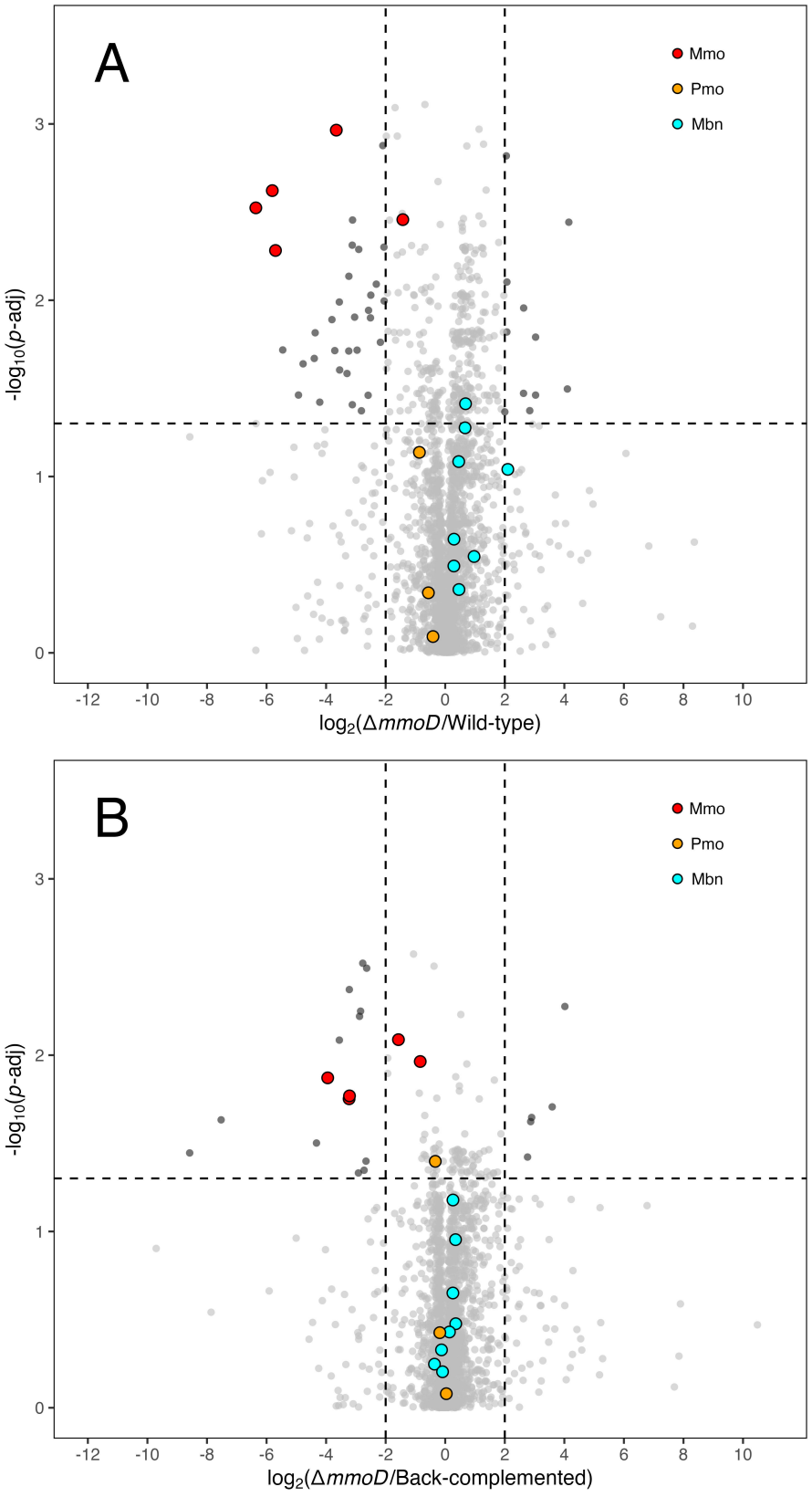

FIG 5 Volcano plot comparing protein intensity of *M. trichosporium* Δ*mmoD* to wild type (A) and Δ*mmoD* to Δ*mmoD* carrying pTJS-*mmoD* (back-complemented strain) (B). Dotted horizontal and vertical lines indicate significant adjusted *P*-value of 0.05 and $|\log_2$ fold change| equal to 2.

in regulating sMMO/pMMO has been known for over 40 years (11, 12), the underlying regulatory mechanism(s), however, is(are) still not completely clear.

Previously, we characterized a mutant of *M. trichosporium* OB3b where *mmoXYBZD* was deleted. In this mutant, *pmoA* expression decreased with increasing copper availability (34). Given this finding, we concluded that MmoD is a key regulatory protein for the copper switch in *M. trichosporium* OB3b. Our results here support this conclusion that MmoD is a critical element for the growth of *M. trichosporium* OB3b Δ*mmoD* in the absence of copper. Unlike our earlier results, however, herein, where we constructed a deletion of *mmoD* only, the expression of neither *pmo* nor *mmo* genes varied with respect to copper (Fig. 2). Thus, although MmoD is important for the growth of *M. trichosporium* OB3b in the absence of copper, we must re-consider our hypothesis that it controls the "copper switch" at the level of transcription.

Intriguingly, no sMMO activity was apparent in *M. trichosporium* OB3b Δ*mmoD* when grown in the absence of copper. In addition, proteomic analysis revealed that the abundance of sMMO polypeptides was significantly lower in Δ*mmoD* than wild-type *M. trichosporium* OB3b and Δ*mmoD*+pTJS-*mmoD* (Fig. 5; Tables S4 and S6). These findings suggest that MmoD may act as a post-transcriptional regulator of sMMO. Such regulation, however, does not appear to extend to pMMO, i.e., neither the expression of *pmoA* nor the presence of pMMO polypeptides was markedly different in *M. trichosporium* OB3b Δ*mmoD,* wild type, or Δ*mmoD*+pTJS-*mmoD* (Fig. 3 and 5; Tables S1 to S6).

With the available data, we can only speculate on the mechanism of such regulation, but at least two general hypotheses can be put forward. First, the translation of *mmo* transcripts may only effectively occur in the presence of MmoD. Second, sMMO polypeptides may be synthesized in *M. trichosporium* OB3b Δ*mmoD* but require MmoD to be assembled to form active sMMO. In this case, the unassembled sMMO polypeptides may be subject to protease attack, e.g., by ClpXP, a bacterial AAA+proteolytic enzyme for damaged/misfolded/unneeded protein degradation (38, 39), leading to the lower abundance of sMMO polypeptides observed in *M. trichosporium* OB3b Δ*mmoD*. This hypothesis has some support as proteases, including ClpXP, are highly expressed in both *M. trichosporium* OB3b Δ*mmoD* and wild type (Tables S1 and S2). This hypothesis is further bolstered by a previous study suggesting that MmoD may act as a protein chaperone to protect MMOH during protein folding (33).

In any event, although the exact role of MmoD in the copper switch is still unclear, it is apparent that the "copper switch" has multiple layers at both transcription and translation to ensure appropriate regulation of pMMO/sMMO. For example, our previous study demonstrates that the copper switch in *M. trichosporium* OB3b involves two TonB-dependent transporters responsible for the uptake of different forms of methanobactin (40, 41). MmoD may serve as an additional regulatory protein to ensure the appropriate response of *M. trichosporium* OB3b to copper.

In addition to the finding that MmoD post-transcriptionally controls sMMO activity, it also appears that it can directly control the expression of methanobactin, a specialized copper uptake system found in *M. trichosporium* OB3b. That is, the expression of *mbnA,* encoding for the precursor polypeptide of MB, was significantly higher in *M. trichosporium* Δ*mmoD* than wild-type *M. trichosporium* OB3b, and UV-Vis spectroscopy indicated the greater presence of MB. Interestingly, although Δ*mmoD* clearly produced more MB than wild type, such increase was not due to the increased expression of other genes in the *mbn* operon, i.e., the expression of *mbnB* and *mbnN* that are critical for the conversion of the precursor polypeptide to mature MB was not significantly different between *M. trichosporium* Δ*mmoD* and wild-type *M. trichosporium* OB3b, nor was the presence of MbnB or MbnN (Fig. S3). Thus, it appears that(i) MB production in *M. trichiosporium* OB3b is primarily controlled by the expression of *mbnA,* (ii) the expression of *mbnA* is controlled by MmoD, and (iii) the expression of other genes in the *mbn* operon can be uncoupled from the expression of *mbnA*.

Previous *in vitro* biochemical study indicates MmoD behaves as an inhibitor for sMMO by competing with MmoB for binding to MMOH, leading to a conformational change of

MMOH (33). In this study, we demonstrate that the lack of MmoD causes the inactivation of sMMO and thereby strongly inhibits the growth of *M. trichosporium* OB3b under no copper condition. Proteomic analysis shows a significantly lower abundance of sMMO polypeptides in cells of Δ*mmoD* as compared to wild type and Δ*mmoD*+pTJS140-*mmoD* (Tables S1 to S6). MmoD clearly has another role other than as an inhibitor of sMMO, likely in facilitating the translation and/or assembly of sMMO polypeptides. Moreover, it should be noted that *in vitro* biochemical analyses found that the inhibition of MmoD on sMMO only occurred when the ratio of MmoD to MMOH was greater than 1 (33). Such a condition is unlikely to occur *in vivo* as the ratio of MmoD to polypeptides of MMOH (MmoX, Y, and Z) is on the order of 0.001 in wild-type *M. trichosporium* OB3b (Table S1). Thus, we conclude that MmoD is involved in controlling the assembly, rather than the catalysis, of sMMO. That is, after the synthesis of sMMO, MmoD is unneeded and will likely be subjected to protease degradation and thus avoid being bound to MMOH. Such an assumption is supported by previous findings showing that the absence of MmoD in purified sMMO (25) as well as the proteomic investigation of *M. capsulatus* Bath showing MmoD polypeptide cannot be detected by LTQ-ORBITRAP mass spectrometry, whereas all sMMO polypeptides (MmoXYZBC) are detected (42).

In conclusion, we show that MmoD is essential for the activity of *M. trichosporium* OB3b in the absence of copper and is involved in regulating the expression of genes needed for methanobactin synthesis. Further study is needed to investigate the roles of MmoD in the biochemistry of sMMO through multiple approaches, such as the expression of sMMO polypeptides with and without MmoD followed by enzymatic assays to elucidate the potential involvement of MmoD in the translation and assembly of sMMO.

MATERIALS AND METHODS

Growth conditions

Wild-type *Methylosinus trichosporium* OB3b, Δ*mmoD*, and Δ*mmoD*+pTJS-*mmoD* (with 25 µg/mL kanamycin) were grown in nitrate mineral salt (NMS) medium (43) in the absence (no added) or presence of copper (1 µM as $CuCl_2$). Methane and air were added at a methane-to-air ratio of 1:2. Cultures were incubated in the dark at 30°C. The solid NMS medium was supplemented with 1.2% agar. Liquid cultures were grown in 250 mL sidearm Erlenmeyer flasks with 20 mL NMS medium with shaking at 200 rpm. Growth was monitored by measuring the optical density at 600 nm (OD_{600}) with a Genesys 20 visible spectrophotometer (Spectronic Unicam, Waltham, MA). Triplicate biological cultures were prepared for all experimental conditions. One-way ANOVA tests were performed for variance analysis of the growth rate and OD_{600} between different transfers and growth conditions of wild-type *M. trichosporium* OB3b, Δ*mmoD*, and Δ*mmoD* with pTJS-*mmoD*. Cultures were harvested at the middle to late exponential phase for RNA isolation and transcriptional analysis of a specific gene expression. *Escherichia coli* was grown in Luria–Bertani broth (LB) at 37°C with or without supplementation of 25 µg/mL kanamycin.

Construction of *M. trichosporium* OB3b Δ*mmoD*

mmoD was knocked out using a previously described protocol (44) with modifications. Briefly, upstream and downstream regions of *mmoD* (arms A and B, respectively) were amplified using the primers listed in Table 1. Arms A and B were digested with the appropriate restriction enzymes and ligated together to form armAB, which was subsequently inserted into pK18mobsacB mobilizable suicide vector (Fig. S1) (45). pK18mobsacB vector with armAB was transferred to *E. coli* Top10 (Invitrogen, Carlsbad, CA). The plasmid was then extracted from transformed *E. coli* Top10 using the Plasmid Mini Kit (Qiagen, Hilden, Germany) following the manufacturer's instructions. The extracted plasmid was then transferred to *E. coli* S17-1 (46). Conjugation of *E. coli* S17-1

carrying the constructed vector with *M. trichosporium* OB3b was performed as described by Martin and Murrell (47). Transconjugants were grown on NMS plates supplemented with 25 µg/mL kanamycin and 10 µg/mL nalidixic acid. One kanamycin-resistant transconjugant colony (generated after 10 d of incubation) was transferred to an NMS plate with kanamycin (25 µg/mL) and incubated for 7 d, and subsequently transferred to an NMS plate with 2.5% sucrose (mass/vol). Sucrose-resistant colonies were generated after a 10-d incubation and were screened for deletion of *mmoD* by colony PCR using checking primers (Table 1). Successful *mmoD* deletion mutant was further confirmed by PCR with DNA extracted from the mutant using the DNeasy PowerSoil Pro Kit (Qiagen, Hilden, Germany) following the manufacturer's instructions.

Back complementation of Δ*mmoD*

mmoD with its native promoter was PCR-amplified using the primer listed in Table 1 and cloned into pTJS140 broad-host-range cloning vector (50). The pTJS140 vector with *mmoD* (pTJS-*mmoD*) was transformed to *E. coli* S17-1. The back complementation strain (Δ*mmoD* carrying pTJS-*mmoD*) was obtained by introducing pTJS-*mmoD* into Δ*mmoD* via conjugation as described above. Δ*mmoD* carrying pTJS-*mmoD* was growing and maintained in NMS medium with 25 µg/mL kanamycin.

RNA isolation and reverse transcription-quantitative PCR

RNA was isolated from biomass in the middle to late exponential growth phase of the first growth iteration of each strain. RNA isolation was performed using a bead-beating procedure followed by column purification using an RNeasy Mini Kit (Qiagen, Hilden, Germany) as described before (51). Genomic DNA was removed from the column with RNase-free DNase (Qiagen, Hilden, Germany) treatment. The absence of genomic

TABLE 1 Primers used in this study

Primer name	Sequence (5′–3′)[a]	Application	Reference
qmmoC_F	TCAATCACCGTTCCCTTGTC	RT-qPCR	This study
qmmoC_R	ATCGCGAGGAATTGTTCTATGT		
qmmoD_F	CGAGCGCTATCAAGCCTATAC	RT-qPCR	This study
qmmoD_R	AAAGTGGCTCAGCACATGA		
qmmoX_F	TCAACACCGATCTSAACAACG	RT-qPCR	(48)
qmmoX_R	TCCAGATTCCRCCCCAATCC		
qpmoA_F	TTCTGGGGCTGGACCTAYTTC	RT-qPCR	(48)
qpmoA_R	CCGACAGCAGCAGGATGATG		
qmbnA_F	TGGAAACTCCCTTAGGAGGAA	RT-qPCR	(34)
qmbnA_R	CTGCACGGATAGCACGAAC		
qmbnB_F	CGTATTCCACGAGGCGAAGA	RT-qPCR	This study
qmbnB_R	GCTTCCCGAGCTTCTCCAAT		
qmbnN_F	GATTTCGCCGAAGTGGAAAA	RT-qPCR	This study
qmbnN_R	GCGTAATGAGCATACATCGG		
Eub-341_F	CCTACGGGAGGCAGCAG	RT-qPCR	(49)
Eub-534_R	ATTACCGCGGCTGCTGGC		
mmoD-armA_F	ATTTTT gaattc GGCACCAAATTCACCATCACCb	Arm PCR	This study
mmoD-armA_R	ATTTTT ggtacc GAACGCATGTCTTTCGCAAT		
mmoD-armB_F	ATTTTT ggtacc TGCTGCGCGAGATCGGAAb	Arm PCR	This study
mmoD-armB_R	ATTTTT aagctt GACGGATGAAGAATTCGAGCTG		
mmoD-check_F[c]	TTATTACGGCACTCCGCTCG	PCR for mutant check	This study
mmoD-check_R[c]	TCAGCTCATAATCGCCGTCC		
mmoD_F	ATTTTT ggtacc GAGTTCCGGCAGCTCTACA	mmoD PCR for back complementation	This study
mmoD-R	ATTTTT gcatgc GAACGAACAGGTTTCTCCGTC		

[a]Y, S, and R are the IUPAC DNA codes for the C/T, C/G, and A/G nucleobases, respectively.
[b]Lowercase letters indicate EcoRI, KpnI, SphI, or HindIII restriction site sequences included in these primers.
[c]Targeting region indicated in Fig. S2.

DNA was confirmed by 16S rRNA gene-targeted PCR with extracted RNA samples as templates. Purified RNA was quantified using a NanoDrop 1000 Spectrophotometer (Thermo Scientific, Wilmington, DE). cDNA was synthesized from 200 ng total RNA using SuperScript III Reverse Transcriptase (Invitrogen, Carlsbad, CA) following the manufacturer's instructions.

RT-qPCR was performed to determine the relative expression of the *pmoA*, *mmoX*, *mmoC*, *mmoD* and *mbnA* in *M. trichosporium* OB3b, Δ*mmoD*, and Δ*mmoD* carrying pTJS-*mmoD* grown in the presence or absence of copper, as well as *mbnB* and *mbnN* in the absence of copper. Primers were designed using the NCBI online primer design tool (http://www.ncbi.nlm.nih.gov/tools/primer-blast/). Primer specificity was checked with the online tool and further verified by PCR, gel electrophoresis, and sequencing. RT-qPCR was performed using the iTaq Universal SYBR Green Supermix (Bio-Rad, Hercules, CA) with 96-well PCR plates on a CFX Connect Real-Time PCR Detection System (Bio-Rad, Hercules, CA). The RT-qPCR program was 95°C for 10 min, followed by 40 cycles of 95°C for 15 s, 56°C for 30 s, and 72°C for 30 s. Melting curves were measured from 65°C to 95°C with increments of 0.5°C and 10 s at each step. The transcription of the targeted genes was determined using cDNA as the template. The transcript levels were calculated by relative quantification using the $2^{-\Delta\Delta Cq}$ method (52) with the 16S rRNA gene as the reference gene (53).

sMMO activity

sMMO activity was measured using resting cells of *M. trichosporium* OB3b, Δ*mmoD*, and Δ*mmoD* carrying pTJS-*mmoD* grown in the absence (no added) of copper and the presence of 1 µM copper. Cells were harvested at the middle to late exponential growth phase of the first growth iteration and resuspended in 1.6 mL NMS medium (without copper) in a 2 mL screw-cap tube. Naphthalene was then added to the cell suspensions and incubated at 30°C for 1 h with shaking at 200 rpm. Fast Blue B (tetrazotized o-dianisidine, 4.21 mM) was subsequently added to the supernatant of the cell suspensions for visualization of the production of napthol from naphthalene, a process that can only be mediated by sMMO and not pMMO (54).

Sample preparation for proteomic analysis

M. trichosporium OB3b, Δ*mmoD*, and Δ*mmoD*+pTJS-*mmoD* grown without copper were collected at the middle to late exponential growth phase of the first growth iteration of each strain for proteomic analysis. Cells were lysed in modified RIPA buffer (2% SDS, 50 mM Tris HCl pH 8, 150 mM NaCl, 1× Roche cOmplete protease inhibitor) using a QSonica sonic probe with the following settings: amplitude 50%, pulse 10 × 1 s, 1 on, 1 off. Extracts were subjected to TCA precipitation according to the method of Jessie et al. (55). Washed protein pellets were solubilized in 500 µL of urea buffer (8 M urea, 150 mM NaCl, 50 mM Tris pH 8, 1× Roche cOmplete protease inhibitor). Protein quantitation was performed using Qubit fluorometry (Invitrogen). Fifty micrograms of each lysate was digested with the protocol as follows: (i) reduction with 15 mM dithiothreitol at 25°C for 30 min followed by alkylation with 15 mM iodoacetamide at 25°C for 45 min in the dark; (ii) digestion with 2.5 µg sequencing grade trypsin (Promega) at 37°C overnight. The final digest volume was amended with 0.5 mL 25 mM ammonium bicarbonate; (iii) the resulting mixture was cooled to 25°C, acidified with formic acid, and desalted using a Waters Oasis HLB solid-phase extraction plate. Eluted samples were then frozen and lyophilized; and (iv) a pooled sample was made by mixing equal amounts of digested material from each sample. This pooled sample was used to generate a gas phase fractionation library.

Mass spectrometry analysis

Data-independent-acquisition chromatogram library generation

One microgram of the pooled sample was analyzed by nano LC-MS/MS with a Waters M-class HPLC system interfaced with ThermoFisher Exploris 480. Peptides were loaded on a trapping column and eluted over a 75-µm analytical column at 350 nL/min where both columns were packed with XSelect CSH C18 resin (Waters). The trapping column was composed of 5-µm particles, and the analytical column contained 2.4-µm particles. The column was heated to 55°C using a column heater (Sonation). The sample was analyzed using 6 × 0.5-h gradients. Six gas-phase fraction injections were acquired for six ranges: 396–502, 496–602, 596–702, 696–802, 796–902, and 896–1,002. Sequentially, full-scan MS data [60,000 full width at half maximum (FWHM) resolution] was followed by 26 × 4 m/z precursor isolation windows, another full scan, and 26 × 4 m/z windows staggered by 2 m/z. The products were acquired at 30,000 FWHM resolution. The automatic gain control (AGC) target was set to 10^6 for both full MS and production data. The maximum ion inject time (IIT) was set to 50 ms for full MS and dynamic mode for products with nine data points required across the peak. The normalized collision energy (NCE) was set to 30.

Sample analysis

Samples were randomized for acquisition. One microgram per sample was analyzed by nano LC/MS with a Waters M-class HPLC system interfaced with ThermoFisher Exploris 480. Peptides were loaded on a trapping column and eluted over a 75 µm analytical column at 350 nL/min; both columns were packed with XSelect CSH C18 resin (Waters); the trapping column contained 5-µm particles, and the analytical column contained 2.4-µm particles. The column was heated to 55°C using a column heater (Sonation). Samples were analyzed using a 0.5-h gradient. The mass spectrometer was operated in a data-independent mode. Sequentially, full scan MS data (60,000 FWHM resolution) from 385–1,015 m/z was followed by 61 × 10 m/z precursor isolation windows; another full scan from 385–1,015 m/z was followed by 61 × 10 m/z windows staggered by 5 m/z; products were acquired at 15,000 FWHM resolution. The maximum ion inject time was set to 50 ms for full MS and dynamic mode for products with nine data points required across the peak; the NCE was set to 30.

Data processing

DIA data were analyzed using Scaffold DIA 3.3.1 (Proteome Software). DIA-MS data files were converted to mzML format using ProteoWizard (3.0.21072). Deconvolution of staggered windows was performed. Analytic samples were aligned based on retention times and individually searched against the Prosit library (DLIB) and the chromatogram/reference library to create a custom EncyclopeDIA library. The digestion enzyme was assumed to be trypsin with a maximum of one missed cleavage site allowed. Peptides identified in each sample were filtered by Percolator to achieve a maximum FDR of 0.01. Individual search results were combined, and peptide identifications were assigned posterior error probabilities and filtered to an FDR threshold of 0.01 by Percolator. Peptide quantification was performed by Encyclopedia (1.12.31). For each peptide, the five highest-quality fragment ions were selected for quantitation. Proteins that contained similar peptides and could not be differentiated based on MS/MS analysis were grouped to satisfy the principles of parsimony. Protein groups with a minimum of two identified peptides were thresholded to achieve a protein FDR of less than 1.0%. The sample *q*-value was set to less than 0.01. Statistical difference in protein intensity between the groups was analyzed by ANOVA. The *P*-value was adjusted using the standard Benjamini and Hochberg procedure, and the proteins with adjusted *P*-value <0.05 were considered statistically significant.

ACKNOWLEDGMENTS

We thank Joshua Sodicoff for help in constructing the ΔmmoD mutant, Jin Chang for providing the pTJS140 vector with kanamycin resistance gene, and Henriette Remmer for assistance with proteomic data collection and analyses.

This research was supported by the U.S. Department of Energy Office of Science (Grant # DE-SC0020174 to J.D.S. and A.A.D.) and the U.S. National Science Foundation (Grant # 1912482 to J.D.S.).

AUTHOR AFFILIATIONS

[1]Department of Civil and Environmental Engineering, University of Michigan, Ann Arbor, Michigan, USA
[2]Roy J. Carver Department of Biochemistry, Biophysics and Molecular Biology, Iowa State University, Ames, Iowa, USA

AUTHOR ORCIDs

Peng Peng http://orcid.org/0000-0001-9982-5210
Alan A. DiSpirito http://orcid.org/0000-0003-3602-6213
Jeremy D. Semrau http://orcid.org/0000-0002-1670-9984

FUNDING

Funder	Grant(s)	Author(s)
National Science Foundation (NSF)	1912482	Jeremy D. Semrau
U.S. Department of Energy (DOE)	DE-SC0020174	Alan A. DiSpirito Jeremy D. Semrau

AUTHOR CONTRIBUTIONS

Peng Peng, Conceptualization, Data curation, Formal analysis, Investigation, Validation, Visualization, Writing – original draft | Junwon Yang, Data curation, Formal analysis, Investigation, Writing – original draft | Alan A. DiSpirito, Conceptualization, Data curation, Formal analysis, Funding acquisition, Writing – review and editing | Jeremy D. Semrau, Conceptualization, Data curation, Formal analysis, Funding acquisition, Investigation, Project administration, Writing – review and editing

DATA AVAILABILITY

Data that supports the findings of this study are available in the supplementary material of this article. In addition, proteomic data are available at the PRIDE database, accession number PXD045741.

ADDITIONAL FILES

The following material is available online.

Supplemental Material

Tables S1 to S6 (AEM01601-23-s0001.xlsx). Proteomic data sets.
Fig. S1 to S4 (AEM01601-23-s0002.docx). General protocols and supplemental data.

REFERENCES

1. Anonymous. 2013. IPCC, 2013: climate change 2013: the physical science basis. In Contribution of working group I to the fifth assessment report of the intergovernmental panel on climate change Cambridge. Univ. Press, Cambridge, United Kingdom and New York, NY, USA.

2. Knittel K, Boetius A. 2009. Anaerobic oxidation of methane: progress with an unknown process. Annu Rev Microbiol 63:311–334. https://doi.org/10.1146/annurev.micro.61.080706.093130
3. Semrau JD, DiSpirito AA, Gu W, Yoon S. 2018. Metals and methanotrophy. Appl Environ Microbiol 84:e02289-17. https://doi.org/10.1128/AEM.02289-17
4. Semrau JD, DiSpirito AA, Yoon S. 2010. Methanotrophs and copper. FEMS Microbiol Rev 34:496–531. https://doi.org/10.1111/j.1574-6976.2010.00212.x
5. Koo CW, Rosenzweig AC. 2021. Biochemistry of aerobic biological methane oxidation. Chem Soc Rev 50:3424–3436. https://doi.org/10.1039/d0cs01291b
6. Banerjee R, Jones JC, Lipscomb JD. 2019. Soluble methane monooxygenase. Annu Rev Biochem 88:409–431. https://doi.org/10.1146/annurev-biochem-013118-111529
7. Colby J, Stirling DI, Dalton H. 1977. The soluble methane monooxygenase of *Methylococcus capsulatus* (Bath). Its ability to oxygenate *n*-alkanes, *n*-alkenes, ethers, and alicyclic, aromatic and heterocyclic compounds. Biochem J 165:395–402. https://doi.org/10.1042/bj1650395
8. Choi D-W, Kunz RC, Boyd ES, Semrau JD, Antholine WE, Han J-I, Zahn JA, Boyd JM, de la Mora AM, DiSpirito AA. 2003. The membrane-associated methane monooxygenase (pMMO) and pMMO-NADH: quinone oxidoreductase complex from *Methylococcus capsulatus* Bath. J Bacteriol 185:5755–5764. https://doi.org/10.1128/JB.185.19.5755-5764.2003
9. Nguyen HH, Shiemke AK, Jacobs SJ, Hales BJ, Lidstrom ME, Chan SI. 1994. The nature of the copper ions in the membranes containing the particulate methane monooxygenase from *Methylococcus capsulatus* (Bath). J Biol Chem 269:14995–15005.
10. van Spanning RJM, Guan Q, Melkonian C, Gallant J, Polerecky L, Flot J-F, Brandt BW, Braster M, Iturbe Espinoza P, Aerts JW, Meima-Franke MM, Piersma SR, Bunduc CM, Ummels R, Pain A, Fleming EJ, van der Wel NN, Gherman VD, Sarbu SM, Bodelier PLE, Bitter W. 2022. Methanotrophy by a *Mycobacterium* species that dominates a cave microbial ecosystem. Nat Microbiol 7:2089–2100. https://doi.org/10.1038/s41564-022-01252-3
11. Burrows KJ, Cornish A, Scott D, Higgins IJ. 1984. Substrate specificities of the soluble and particulate methane mono-oxygenases of *Methylosinus trichosporium* OB3b. Microbiology 130:3327–3333. https://doi.org/10.1099/00221287-130-12-3327
12. Stanley SH, Prior SD, Leak DJ, Dalton H. 1983. Copper stress underlies the fundamental change in intracellular location of methane monooxygenase in methane-oxidizing organisms: studies in batch and continuous cultures. Biotechnol Lett 5:487–492. https://doi.org/10.1007/BF00132233
13. Ross MO, MacMillan F, Wang J, Nisthal A, Lawton TJ, Olafson BD, Mayo SL, Rosenzweig AC, Hoffman BM. 2019. Particulate methane monooxygenase contains only mononuclear copper centers. Science 364:566–570. https://doi.org/10.1126/science.aav2572
14. Koo CW, Tucci FJ, He Y, Rosenzweig AC. 2022. Recovery of particulate methane monooxygenase structure and activity in a lipid bilayer. Science 375:1287–1291. https://doi.org/10.1126/science.abm3282
15. Balasubramanian R, Smith SM, Rawat S, Yatsunyk LA, Stemmler TL, Rosenzweig AC. 2010. Oxidation of methane by a biological dicopper centre. Nature 465:115–119. https://doi.org/10.1038/nature08992
16. Rosenzweig AC, Sazinsky MH. 2006. Structural insights into dioxygen-activating copper enzymes. Curr Opin Struct Biol 16:729–735. https://doi.org/10.1016/j.sbi.2006.09.005
17. Cao L, Caldararu O, Rosenzweig AC, Ryde U. 2018. Quantum refinement does not support dinuclear copper sites in crystal structures of particulate methane monooxygenase. Angew Chem Int Ed Engl 57:162–166. https://doi.org/10.1002/anie.201708977
18. Lieberman RL, Rosenzweig AC. 2005. Crystal structure of a membrane-bound metalloenzyme that catalyses the biological oxidation of methane. Nature 434:177–182. https://doi.org/10.1038/nature03311
19. Chan SI, Yu S-F. 2008. Controlled oxidation of hydrocarbons by the membrane-bound methane monooxygenase: the case for a tricopper cluster. Acc Chem Res 41:969–979. https://doi.org/10.1021/ar700277n
20. Chan SI, Lu Y-J, Nagababu P, Maji S, Hung M-C, Lee MM, Hsu I-J, Minh PD, Lai J-H, Ng KY, Ramalingam S, Yu S-F, Chan MK. 2013. Efficient oxidation of methane to methanol by dioxygen mediated by tricopper clusters. Angew Chem Int Ed Engl 52:3731–3735. https://doi.org/10.1002/anie.201209846
21. Martinho M, Choi DW, Dispirito AA, Antholine WE, Semrau JD, Münck E. 2007. Mössbauer studies of the membrane-associated methane monooxygenase from *Methylococcus capsulatus* Bath: evidence for a diiron center. J Am Chem Soc 129:15783–15785. https://doi.org/10.1021/ja077682b
22. Rosenzweig AC, Nordlund P, Takahara PM, Frederick CA, Lippard SJ. 1995. Geometry of the soluble methane monooxygenase catalytic diiron center in two oxidation states. Chem Biol 2:409–418.
23. Rosenzweig AC, Frederick CA, Lippard SJ, Nordlund P. 1993. Crystal structure of a bacterial non-haem iron hydroxylase that catalyses the biological oxidation of methane. Nature 366:537–543. https://doi.org/10.1038/366537a0
24. Lipscomb JD. 1994. Biochemistry of the soluble methane monooxygenase. Annu Rev Microbiol 48:371–399. https://doi.org/10.1146/annurev.mi.48.100194.002103
25. Fox BG, Froland WA, Dege JE, Lipscomb JD. 1989. Methane monooxygenase from *Methylosinus trichosporium* OB3b: purification and properties of a three-component system with high specific activity from a type II methanotroph. J Biol Chem 264:10023–10033.
26. Lund J, Woodland MP, Dalton H. 1985. Electron transfer reactions in the soluble methane monooxygenase of *Methylococcus capsulatus* (Bath). Eur J Biochem 147:297–305. https://doi.org/10.1111/j.1432-1033.1985.tb08750.x
27. Merkx M, Kopp DA, Sazinsky MH, Blazyk JL, Müller J, Lippard SJ. 2001. Dioxygen activation and methane hydroxylation by soluble methane monooxygenase: a tale of two irons and three proteins. Angew Chem Int Ed 40:2782–2807. https://doi.org/10.1002/1521-3773(20010803)40:15<2782::AID-ANIE2782>3.0.CO;2-P
28. Tinberg CE, Lippard SJ. 2011. Dioxygen activation in soluble methane monooxygenase. Acc Chem Res 44:280–288. https://doi.org/10.1021/ar1001473
29. Lee SJ, McCormick MS, Lippard SJ, Cho U-S. 2013. Control of substrate access to the active site in methane monooxygenase. Nature 494:380–384. https://doi.org/10.1038/nature11880
30. Froland WA, Andersson KK, Lee SK, Liu Y, Lipscomb JD. 1992. Methane monooxygenase component B and reductase alter the regioselectivity of the hydroxylase component-catalyzed reactions. A novel role for protein-protein interactions in an oxygenase mechanism. J Biol Chem 267:17588–17597.
31. LaFleur TL, Hossain A, Salis HM. 2022. Automated model-predictive design of synthetic promoters to control transcriptional profiles in bacteria. Nat Commun 13:5159. https://doi.org/10.1038/s41467-022-32829-5
32. Merkx M, Lippard SJ. 2002. Why Orfy?: CHARACTERIZATION OF MMOD, A LONG OVERLOOKED COMPONENT OF THE SOLUBLE METHANE MONOOXYGENASE FROM METHYLOCOCCUS CAPSULATUS (BATH) J Biol Chem 277:5858–5865. https://doi.org/10.1074/jbc.M107712200
33. Kim H, An S, Park YR, Jang H, Yoo H, Park SH, Lee SJ, Cho U-S. 2019. MMOD-induced structural changes of hydroxylase in soluble methane monooxygenase. Sci Adv 5:eaax0059. https://doi.org/10.1126/sciadv.aax0059
34. Semrau JD, Jagadevan S, DiSpirito AA, Khalifa A, Scanlan J, Bergman BH, Freemeier BC, Baral BS, Bandow NL, Vorobev A, Haft DH, Vuilleumier S, Murrell JC. 2013. Methanobactin and MmoD work in concert to act as the 'copper‐switch' in methanotrophs. Environ Microbiol 15:3077–3086. https://doi.org/10.1111/1462-2920.12150
35. Yuan H, Collins ML, Antholine WE. 1999. Type 2 Cu^{2+} in pMMO from *Methylomicrobium album* BG8. Biophys J 76:2223–2229. https://doi.org/10.1016/S0006-3495(99)77378-9
36. Im J, Lee S-W, Yoon S, Dispirito AA, Semrau JD. 2011. Characterization of a novel facultative *Methylocystis* species capable of growth on methane, acetate and ethanol. Environ Microbiol Rep 3:174–181. https://doi.org/10.1111/j.1758-2229.2010.00204.x
37. Kits KD, Kalyuzhnaya MG, Klotz MG, Jetten MSM, Op den Camp HJM, Vuilleumier S, Bringel F, Dispirito AA, Murrell JC, Bruce D, Cheng J-F, Copeland A, Goodwin L, Hauser L, Lajus A, Land ML, Lapidus A, Lucas S, Médigue C, Pitluck S, Woyke T, Zeytun A, Stein LY. 2013. Genome sequence of the obligate gammaproteobacterial methanotroph *Methylomicrobium album* strain BG8. Genome Announc 1:e0017013. https://doi.org/10.1128/genomeA.00170-13

38. Olivares AO, Baker TA, Sauer RT. 2018. Mechanical protein unfolding and degradation. Annu Rev Physiol 80:413–429. https://doi.org/10.1146/annurev-physiol-021317-121303
39. Gu W, Semrau JD. 2017. Copper and cerium-regulated gene expression in *Methylosinus trichosporium* OB3b. Appl Microbiol Biotechnol 101:8499–8516. https://doi.org/10.1007/s00253-017-8572-2
40. Peng P, Gu W, DiSpirito AA, Semrau JD. 2022. Multiple mechanisms for copper uptake by *Methylosinus trichosporium* OB3b in the presence of heterologous methanobactin. mBio 13:e0223922. https://doi.org/10.1128/mbio.02239-22
41. Peng P, Kang-Yun CS, Chang J, Gu W, DiSpirito AA, Semrau JD. 2022. "Two Tonb-dependent transporters in Methylosinus Trichosporium Ob3B are responsible for uptake of different forms of Methanobactin and are involved in the Canonical 'copper switch'" Appl Environ Microbiol 88:e0179321. https://doi.org/10.1128/AEM.01793-21
42. Larsen Ø, Karlsen OA. 2016. Transcriptomic profiling of *Methylococcus capsulatus* (Bath) during growth with two different methane monooxygenases. Microbiologyopen 5:254–267. https://doi.org/10.1002/mbo3.324
43. Whittenbury R, Phillips K, Wilkinson J. 1970. Enrichment, isolation and some properties of methane-utilizing bacteria. Microbiology 61:205–218. https://doi.org/10.1099/00221287-61-2-205
44. Welander PV, Summons RE. 2012. Discovery, taxonomic distribution, and phenotypic characterization of a gene required for 3-methylhopanoid production. Proc Natl Acad Sci U S A 109:12905–12910. https://doi.org/10.1073/pnas.1208255109
45. Schäfer A, Tauch A, Jäger W, Kalinowski J, Thierbach G, Pühler A. 1994. Small mobilizable multi-purpose cloning vectors derived from the *Escherichia coli* plasmids pK18 and pK19: selection of defined deletions in the chromosome of *Corynebacterium glutamicum*. Gene 145:69–73. https://doi.org/10.1016/0378-1119(94)90324-7
46. Simon R. 1984. High frequency mobilization of gram-negative bacterial replicons by the *in vitro* constructed Tn*5*-Mob transposon. Mol Gen Genet 196:413–420. https://doi.org/10.1007/BF00436188
47. Martin H, Murrell JC. 1995. Methane monooxygenase mutants of *Methylosinus trichosporium* constructed by marker-exchange mutagenesis. FEMS Microbiol Lett 127:243–248. https://doi.org/10.1111/j.1574-6968.1995.tb07480.x
48. Knapp CW, Fowle DA, Kulczycki E, Roberts JA, Graham DW. 2007. Methane monooxygenase gene expression mediated by methanobactin in the presence of mineral copper sources. Proc Natl Acad Sci U S A 104:12040–12045. https://doi.org/10.1073/pnas.0702879104
49. Muyzer G, de Waal EC, Uitterlinden AG. 1993. Profiling of complex microbial populations by denaturing gradient gel electrophoresis analysis of polymerase chain reaction-amplified genes coding for 16S rRNA. Appl Environ Microbiol 59:695–700. https://doi.org/10.1128/aem.59.3.695-700.1993
50. Smith TJ, Slade SE, Burton NP, Murrell JC, Dalton H. 2002. Improved system for protein engineering of the hydroxylase component of soluble methane monooxygenase. Appl Environ Microbiol 68:5265–5273. https://doi.org/10.1128/AEM.68.11.5265-5273.2002
51. Peng P, Zheng Y, Koehorst JJ, Schaap PJ, Stams AJM, Smidt H, Atashgahi S, Zhou N-Y. 2017. Concurrent haloalkanoate degradation and chlorate reduction by *Pseudomonas chloritidismutans* AW-1^T. Appl Environ Microbiol 83:e00325-17. https://doi.org/10.1128/AEM.00325-17
52. Schmittgen TD, Livak KJ. 2008. Analyzing real-time PCR data by the comparative C^T method. Nat Protoc 3:1101–1108. https://doi.org/10.1038/nprot.2008.73
53. Kalidass B, Ul-Haque MF, Baral BS, DiSpirito AA, Semrau JD. 2015. Competition between metals for binding to methanobactin enables expression of soluble methane monooxygenase in the presence of copper. Appl Environ Microbiol 81:1024–1031. https://doi.org/10.1128/AEM.03151-14
54. Brusseau GA, Tsien HC, Hanson RS, Wackett LP. 1990. Optimization of trichloroethylene oxidation by methanotrophs and the use of a colorimetric assay to detect soluble methane monooxygenase activity. Biodegradation 1:19–29. https://doi.org/10.1007/BF00117048
55. Jessie K, Hashim OH, Rahim ZHA. 2008. Protein precipitation method for salivary proteins and rehydration buffer for two-dimensional electrophoresis. Biotechnology 7:686–693. https://doi.org/10.3923/biotech.2008.686.693